Research Square

Preprints are preliminary reports that have not undergone peer review.
They should not be considered conclusive, used to inform clinical practice,
or referenced by the media as validated information.

# AIoT-Driven Closed-Loop Thermal Regulation for Photopolymerization: A CNN–TCN Edge-Computing Framework

**Kai-Chao Yao**
National Changhua University of Education
**Sumei Chiang**
67848124su@gmail.com

National Changhua University of Education
**Po-Yu Kuo**
National Yunlin University of Science and Technology
**Wei-Hao Ni**
National Yunlin University of Science and Technology

**Article**

**Keywords:** AIoT, Edge AI, Closed-Loop Control, CNN–TCN, Thermal Prediction

**Posted Date:** August 13th, 2026

**DOI:** https://doi.org/10.21203/rs.3.rs-10522376/v1

**License:** This work is licensed under a Creative Commons Attribution 4.0 International License.
Read Full License

**Additional Declarations:** No competing interests reported.

# AIoT-Driven Closed-Loop Thermal Regulation for Photopolymerization: A CNN–TCN Edge-Computing Framework

Kai-Chao Yao [1], Sumei Chiang [1*], Po-Yu Kuo [2], Wei-Hao Ni [3]
[1.] Department of Electrical and Mechanical Technology, National Changhua University of Education, Taiwan.
[2.] Department of Electronics Engineering, National Yunlin University of Science and Technology, Taiwan.
[3.] Department of Mechanical Engineering, National Yunlin University of Science and Technology, Taiwan.
[*] Corresponding Author: Email: 67848124su@gmail.com.

## Affiliations:

**Kai-Chao Yao** was born in Changhua, Taiwan, in 1971. He obtained a Bachelor's and Master's degree in Electrical Engineering from the University of New Haven and a *Ph.D.* in Electrical and Computer Engineering from Wichita State University in the United States in 2000. He is a professor in the Department of Electrical and Mechanical Technology at NCUE, Taiwan. His research interests include electrical engineering, sensors, and virtual instrument technology.

**Sumei Chiang** was born in Hubei, China, in 1979. She received her MS degree from MDU, Taiwan. She is currently a Ph.D. candidate in the Department of Electrical and Mechanical Technology at NCUE, Taiwan. She was an assistant professor in the Department of Leisure and Health Studies at MDU. Her research interests include nail art, sensors, virtual reality, and interdisciplinary methodologies.

**Po-Yu Kuo** was born in Taichung, Taiwan, in 1980. He received his MS and *Ph.D.* degrees in Electrical Engineering from the University of Texas at Dallas in 2006 and 2011, respectively. He is a professor at the Department of Electronic Engineering at NYUST, Taiwan. His research interests include analog circuits, power management circuits, and biosensor applications.

**Wei-Hao Ni** was born in 2002 in Taipei, Taiwan. He holds a bachelor's degree from Southern Taiwan University of Science and Technology, majoring in mechanical engineering. He is a master's degree student in mechanical engineering at NYUST. His research focuses on control technology for self-driving electric buses, primarily in automation control, sensors, and vehicle dynamics.

**ABSTRACT**

Effective thermal management in photopolymerization processes is essential for ensuring material integrity, product quality, and modern nail-gel curing applications. Conventional UV-LED curing systems operate in an open-loop mode, lacking thermal feedback, resulting in uncontrolled temperature fluctuations and inconsistent curing outcomes. This study introduces a Nail Curing Intelligent Testing System (NCITS) that integrates a 1D CNN and a TCN system for real-time thermal prediction and regulation. Although validated through gel nail curing

experiments, the NCITS is designed as a representative demonstrator for controlling exothermic photopolymerization in laboratory-scale prototype contexts, including additive coatings and composite curing. The system interprets thermal dynamics via learned derivative features, enabling predictive intervention before thresholds are exceeded. Experimental results demonstrate peak temperature reductions of up to 35% while maintaining curing efficacy/quality. Compared with PID control, NCITS reduces overshoot by 39.7%, improves settling time by 12.5%, and lowers *RMSE* by 46.6%. Deployment on edge devices with 8-bit quantization achieves 4.2× model compression and inference latencies of 23.4–45.6 ms, confirming its suitability for real-time environments. This research demonstrates potential applicability in small-scale intelligent thermal regulation systems, providing a scalable pathway for the cosmetics industry.

**Keywords:** AIoT, Edge AI, Closed-Loop Control, CNN–TCN, Thermal Prediction.

# 1 Introduction

## 1.1 Problem Statement and Research Motivation

Precise thermal management during photopolymerization is a critical technical challenge [1-2]. Excessive heat generation in UV curing can induce material degradation, alter mechanical properties, and introduce safety concerns. Conventional UV-LED curing systems typically operate in an open-loop configuration without real-time thermal feedback, resulting in temperature overshoot and unstable curing dynamics that compromise polymerization consistency [3–5]. Recent advances in Artificial Intelligence of Things (AIoT) technologies have enabled connected sensing systems capable of real-time data acquisition and embedded analysis [6–7]. While such developments have enhanced monitoring capabilities, active closed-loop thermal regulation in small-scale UV-curing platforms remains underexplored. The nonlinear and time-dependent characteristics of exothermic photopolymerization reactions require predictive rather than purely reactive control strategies.

To address this issue, this study proposes the "Nail Curing Intelligent Testing System (NCITS)", a closed-loop thermal regulation framework integrating a hybrid 1D Convolutional Neural Network (CNN) and Temporal Convolutional Network (TCN). The model extracts short-term thermal gradient features and temporal dependencies to predict near-future temperature trends, enabling anticipatory power modulation before critical thresholds are exceeded. The system is implemented and validated on a controlled UV gel curing platform to evaluate temperature tracking accuracy, overshoot suppression, and dynamic stability. Accordingly, the primary objective of this study is to experimentally verify the feasibility of an AI-assisted closed-loop thermal control mechanism for UV photopolymerization under controlled laboratory conditions.

## 1.2 Related Works

### 1.2.1 AIoT in Aesthetic Innovation and Research Gaps.

The integration of AI with the IoT creates AIoT, elevating devices from data collectors to intelligent systems [8-10]. It uses machine learning for real-time decisions and personalized services [11-13]. Applications exist in cosmetics for simulations and diagnostics [14-19], and in manufacturing for monitoring, but real-time closed-loop control, especially for photopolymerization, is unexplored. Studies such as those on aquaculture monitoring lack integrated control [20-21]. This study develops an AIoT closed-loop platform for coordinated temperature- and image-based recognition control, investigating thermal behavior in gel nail-curing materials.

### 1.2.2 Composition and Characteristics of Gel Nail Materials.

Gel nail systems consist of sequential layers—base coat, color gel, builder gel, and sealer coat—each serving distinct functions [22-23]. The base coat uses low-viscosity, high-permeability formulations to improve adhesion [24]. Color gels depend on medium viscosity and pigment dispersion, though high pigment levels reduce photoinitiator content [25]. Builder gels provide strength through high viscosity, thixotropy, and crosslink density, while the sealer coat ensures transparency, gloss, and durability [26-27]. During curing, exothermic polymerization raises temperatures, sometimes causing burning sensations. UV-LED wavelength (365–420 nm), lamp power, and gel properties influence heat release; builder and sealer gels generate the greatest rise, while base and color gels contribute minimally [22].

### 1.2.3 A CNN-Based Framework for Intelligent Thermal Monitoring.

Accurately predicting temperature during gel curing requires analyzing multivariate time-series data. Traditional machine learning often fails due to reliance on manual feature engineering. In contrast, 1-D CNN and TCN architectures excel at automatically learning discriminative features from raw temporal signals, capturing localized patterns critical for forecasting [28-29]. Benchmark studies confirm the robust generalization and computational efficiency of these models for short-term sequences, making them ideal for real-time use [30-31].

This study employs a 1-D CNN and TCN system to address thermal overshoot. The system processes real-time sensor data to detect instantaneous temperature spikes and predict short-term thermal trends. Its predictive output integrates with an AIoT-based closed-loop control system, enabling proactive UV-LED power regulation to prevent overheating.

### 1.2.4 Thermal Control in Cosmetic Manufacturing.

Traditional thermal control has relied predominantly on PID controllers, which, despite their widespread adoption, suffer from inherent limitations in nonlinear, time-varying processes [32-33]. The PID controllers exhibit poor performance in photopolymerization applications due to the highly nonlinear relationship between UV intensity and thermal response [34]. Advanced control strategies, including model predictive control and adaptive control, have shown promise but require accurate process models that are challenging to obtain due to the complexity of

polymerization kinetics. Compared with the conventional PID control approach [34-36], the proposed method integrates short-term feature extraction and temporal memory modeling. While PID is effective for linear systems, the nonlinear thermal response during UV curing motivates data-driven compensation.

This study uses UV gel nail polish curing as a control platform. Interoperability is achieved through standardized sensor protocols ($DHT_{22}$, $PT_{100}$), transparency is ensured through real-time cloud logging, and decentralized decision-making is implemented using a hybrid 1D-CNN and TCN model deployed at the edge. Cloud synchronization supports not only remote monitoring but also cluster management of curing stations.

# 2 Methodology

## 2.1 Development of an AIoT Closed-Loop Control System for the Photopolymerization Process.

The NCITS system was developed for real-time thermal regulation in photopolymerization. It integrates three modules: (1) a UV-LED curing unit (BQ-3T, 36 W, 365–420 nm) with PWM power control (0–100% in 1% increments) and embedded temperature sensing ($DHT_{22}$, ±0.2 °C; $PT_{100}$ thermocouples with three-point calibration); (2) an edge computing controller (Arduino Uno, 10-bit ADC, 1 kHz sampling) implementing a hybrid learning model combining a four-layer 1D-CNN for local feature extraction and a TCN with dilation factors of 1, 2, 4, and 8 for long-range temporal dependencies; and (3) cloud integration via Wi-Fi/5G for real-time data logging, parameter synchronization, and anomaly detection.

**(1)** UV-LED curing module. The curing platform consists of the LED source, gel nail sample stage, and embedded thermocouple. Surface temperature is continuously monitored and transmitted to the controller for closed-loop regulation.

(2) Edge-based learning controller. The hybrid CNN–TCN model generates thermal predictions, which are converted into power correction signals to adjust LED intensity. This design minimizes overshoot, reduces settling time, and improves tracking accuracy. Stability is maintained by constraining the nonlinear mapping within predefined power limits.

(3) Cloud connectivity. Cloud services provide supportive infrastructure for monitoring and record management. All thermal control computations are executed locally at the edge device to ensure real-time responsiveness.

## 2.2 A Physics-Informed Hybrid 1D-CNN and TCN Architecture for Interpretable Thermal Feature Extraction.

The control algorithm for this experiment operates in three phases: (1) Feature extraction using 1D-CNN kernels designed to approximate temporal derivatives; (2) Temporal pattern recognition using dilated convolutions in the TCN system; and (3) Control signal generation

using the physics-informed law. The algorithm executes with 5-second control intervals, maintaining temperature within ±0.5 °C of the target trajectory.

A hybrid 1D-CNN and TCN system is employed as a dedicated feature extractor for real-time thermal analysis. The model is explicitly designed to quantify the physical dynamics of the exothermic polymerization process, transforming raw temperature data into interpretable control signals. Given a temperature time series $x(t)$, the convolution operation is defined as:

$$fk(t) = \sum_{i=0}^{L-1} \mathrm{w}_k\,(i)x\left(t + i - \left[\frac{L+1}{2}\right]\right) \quad (1)$$

Where $f_k(t)$ is the output of the $k^{th}$ learned kernel at time $t$, $w_k(i)$ is the $k^{th}$ learned kernel with a receptive field of length $L$, and $x(\cdot)$ is the input temperature sequence. The core innovation lies in the direct interpretation of the CNN's outputs. The first-layer kernels are engineered to approximate the first and second-order temporal derivatives of the temperature signal:

$$f_1(t) \approx \frac{dT}{dt}, \quad f_2(t) \approx \frac{d^2T}{dt^2} \quad (2)$$

Here, $f_1(t)$, the thermal rise rate, quantifies the speed of the reaction, while $f_2(t)$, the thermal acceleration, acts as an early warning indicator for sudden heat spikes; $T$ is the temperature signal. These physically meaningful features are fed directly into a transparent control law that modulates the LED curing power:

$$P(t) = P_0 - \alpha f_1(t) - \beta f_2(t) \quad (3)$$

Where $P(t)$ is instantaneous UV-LED irradiance (control signal); $P_0$ is the baseline irradiance; $\alpha$ and $\beta$ are adaptive gains. This proactive strategy enables the system to reduce power in response to the rate of temperature change, preventing thermal overshoot rather than merely reacting to it.

**2.3 Theoretical Model and Convergence Analysis.**

**2.3.1 Convergence Analysis of the Hybrid 1D-CNN and TCN Architecture.**

The hybrid 1D-CNN and TCN system is designed to extract multi-level temporal features from temperature time-series data. Its mathematical formulation is as follows: Let the input temperature sequence be $X = [x_1, x_2, \ldots, x_T]^T$. After $L$ convolutional layers, the feature map $\mathbf{H}(l)$ at layer $l$ can be expressed as:

$$\mathbf{H}^{(l)} = \sigma\left(\mathbf{W}^{(l)} * \mathbf{H}^{(l-1)} + b^{(l)}\right) \quad (4)$$

Where $\mathbf{H}^{(l)}$ is the feature map at layer $l$; $*$ denotes the 1D causal convolution operation; $\mathbf{W}^{(l)}$is the 1-D causal convolution kernel at layer $l$;$b^{(l)}$is the bias vector at layer $l$, and $\sigma$ is the activation function (ReLU in this study). The TCN expands the receptive field through dilated convolution, with the output at layer $l$ given by:

$$\mathbf{H}^{(l)}(t) = \sum_{k=1}^{k} \mathbb{W}^{(l)}\,(k) \cdot \mathbf{H}^{(l-1)}\,(t - d \cdot k) \quad (5)$$

Where $\mathbf{W}^{(l)}(k)$ is the $k^{th}$ filter weight in the dilated convolution at layer $l$; $d$ is the dilation factor, which grows exponentially with network depth; $k$ is the kernel size.

**1) Convergence Proof**

According to statistical learning theory, when the number of training samples $N$ is sufficiently large, and the model complexity is controlled, the generalization error $\epsilon_{gen}$ of the hybrid CNN and TCN system satisfies the following bound:

$$\epsilon_{gen} \leq \hat{0}\left(\sqrt{\frac{v}{N}}\right) + \epsilon_{opt} \quad (6)$$

Where $v$ is the $VC$-dimension of the hybrid CNN-TCN model, $\epsilon_{gen}$ is the generalization error, $\epsilon_{opt}$ is the optimal approximation error, and $N$ is the number of training samples. Due to the residual connections and regularization design of the TCN, gradient flow remains stable during training, and the loss function $L(\theta)$ satisfies Lipschitz continuity, ensuring convergence of the gradient descent algorithm to a local optimum.

**2.3.2 Lyapunov Stability Analysis of the Closed-Loop Control System.**

To achieve precise thermal management, the hybrid CNN and TCN system is embedded in a closed-loop control system. In this study, we define the system state vector as: $s(t) = [T(t), T'(t)]^T$, where $T(t)$ is the temperature and $T'(t)$ is the rate of change. The system state vector can be modeled as:

$$\dot{s}(t) = \mathbf{A}\mathrm{s}(t) + \mathbf{B}u(t) + d(t) \quad (7)$$

Where **A** and **B** are system matrices, $u(t)$ is the control input (UV-LED power), and $d(t)$ is a bounded external disturbance. The control law is designed as:

$$u(t) = -\mathbf{K} \cdot \Phi(s(t); \Theta) \quad (8)$$

Where **K** is the feedback gain matrix, $\Phi(\cdot;\theta)$ is the CNN feature extraction function, and $\theta$ represents trained network weights.

**2). Theory of closed-loop stability**

Khalil [35] indicated that there exists a positive definite matrix **P** satisfying the following linear matrix inequality:

$$\mathbf{A}^T\mathbf{P} + \mathbf{P}\mathbf{A} - 2\mathbf{P}\mathbf{B}\mathbf{K} < 0 \quad (9)$$

Then, the closed-loop system is asymptotically stable in the Lyapunov sense; i.e., there exists a Lyapunov function $V(s) = s^{\mathrm{T}}\mathbf{P}s$ such that $V'$<0, where **P** is the symmetric positive-definite solution matrix of the Lyapunov equation, and the symbol < 0 presents a negative-definite matrix inequality.

**2.3.3 Convergence Rate and the Error Bound Estimation.**

During model training, the Adam optimizer is employed, and the following theorem characterizes its convergence rate. Assuming the loss function $L$ is $\mu$-strongly convex and $L$-smooth, then, after $T$ iterations, the Adam algorithm satisfies:

$$L(\Theta_T) - L(\Theta^*) \leq \frac{D^2}{2T} + \frac{\sigma^2}{\sqrt{T}} \quad (10)$$

Where $\theta_T$ is the parameter set after $T$ Adam iterations; $\theta^*$ is the global minimizer of $L$; $D$ is the diameter of the parameter space, and $\sigma^2$ is the variance of gradient noise. In this experiment, the

training set contains $N = 5000$ samples, with a batch size of 32. The loss converges to a stable region after 200 epochs, validating the practical value of this theoretical bound on real data.

**2.3.4 Key Variables, Parameter Setting, and Performance Evaluation.**

In this study, the system processes thermal images for spatial heat distribution and time-series data using a hybrid 1D-CNN and TCN system, which utilizes temporal patterns, with feature fusion enabling comprehensive state estimation. Trained on 5000 thermal images and 1200 time-series samples across four gel types, the model achieved a validation accuracy of 95% with minimal overfitting. Performance evaluation reveals that the temperature prediction achieved a 0.94 $R^2$ score with a 0.89 °C *RMSE*, while critical temperature rise detection ($\Delta T \geq 3$ °C) yielded a 0.96 $F_1$-score and 0.98 ROC-AUC. Deployment on edge devices demonstrated practical viability, with 8-bit quantization yielding 4.2 × model compression, and inference latencies of 23.4~45.6 ms, suitable for real-time control.

The NCITS system operated with predefined parameters, including an initial temperature of 25 °C, a critical threshold of +3 °C, and control intervals of 5 seconds. These configurations are expected to provide reproducible thermal management while simulating commercial curing conditions, establishing a robust foundation for automated gel nail applications. The results are presented in Table 1.

**Table 1**. Key variables and preset parameters of the AIoT closed-loop control system-NCITS.

| Items | Default Value | Description |
|---|---|---|
| Initial temperature (T0) | 25 °C | Experimental starting temperature at room temperature |
| Critical temperature rise ΔT | +3 °C | Trigger point for starting the cooling mechanism |
| Cooling range | -2 °C | The system automatically adjusts the cooling range |
| Irradiation time | 60 sec/120 sec | Simulate common modes of commercial UV-LED nail lamps |
| Light source power | 36W（BQ-3T UV LED） | Fixed optical power used in the experiment |
| Sensing device | $DHT_{22}$ Temperature sensor<br>$PT_{100}$, K Thermocouple ±0.2 °C | Measure gel surface and ambient temperature |
| Control module | Arduino Uno | Automatic adjustment and data collection |
| Data analysis | LabVIEW 2025 | Real-time display of temperature change curve |
| Test subject | Standard nail sample | Eliminate interference from human body differences |
| Cooling interval | 5 seconds | Cooling control cycle |

**2.4 Schematic Design of the NCITS.**

The NCITS integrates a UV-LED (BQ-3T, 36W), $DHT_{22}$ (0.2°C), $PT_{100}$, and an Arduino Uno controller (see Table 1 for details). For readers' convenience, the research framework of the NCITS is shown in **Fig. 1.**

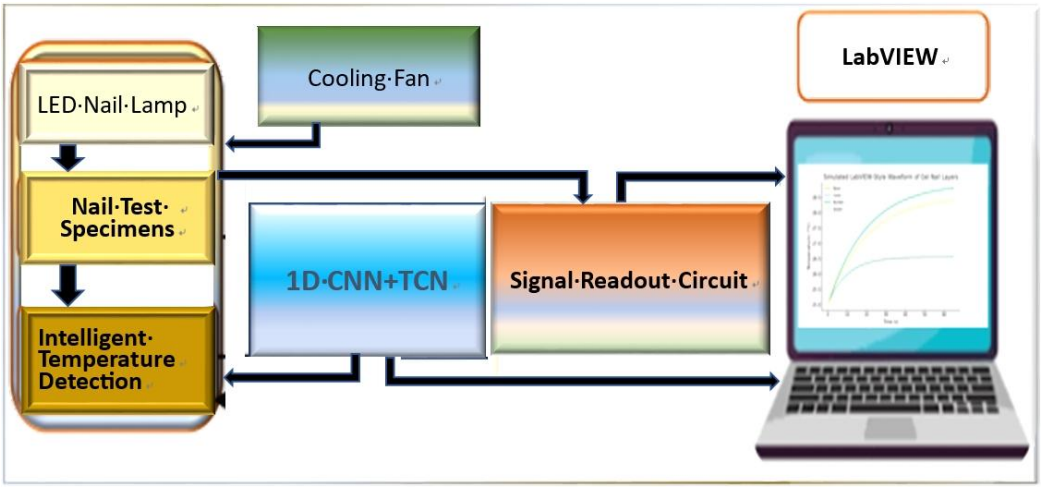
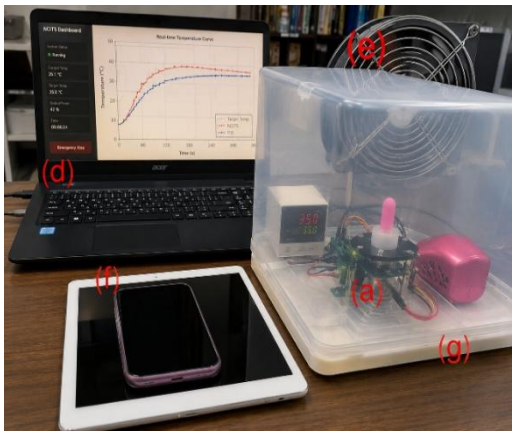
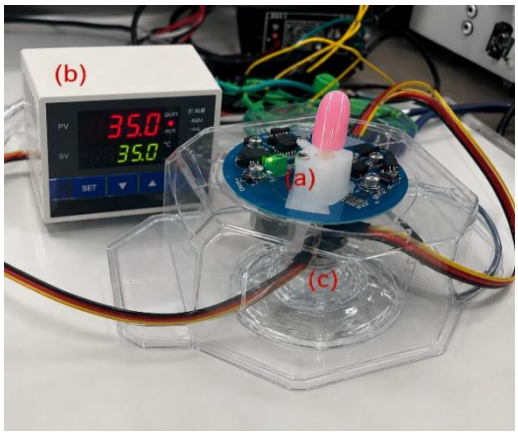



**Fig. 1**. The research framework of the NCITS.

### 2.5 AIoT Gel Nail Experimental Apparatus.

This study employs an experimental methodology. The configuration of the AIoT-based "Gel Nail Curing Testing System" (GNCTS) experimental setup is illustrated in Figure 2.




| **Fig 2** (A) | **Fig 2** (B) |
|---|---|

**Fig 2.** Experimental Layout of the Gel Nail Curing Testing System: (a) Nail gel module, (b) Constant temperature device and temperature controller, (c) Arduino unit and LED light, (d) Microcomputer (installed with LabVIEW 2025), (e) Cooling fan, (f) Smartphone camera, (g) UV LED Gel Nail light.

## 3 Results and Discussion

This study investigated UV-LED curing using artificial nail tips under both uncontrolled and AIoT-controlled conditions ($n_1$ = 30, $n_2$ = 60). A 36W LED cured each layer for 60 s. The AIoT system reduced power when $\Delta T \geq 3$ °C, lowering the temperature by 2 °C per 5-second cycle. A $DHT_{22}$ sensor recorded peak temperatures and timestamps to analyze the thermal response of each layer (Table 2).

**Table 2**. Sensor measurements for the four gel layers.

| Time(s) | Without temperature control (°C) | With AIoT closed-loop control (°C) | Notes |
|---|---|---|---|
| Base Coat | | | |
| 0 | 25.0 | 25.0 | Initial ambient temperature |
| 5 | 25.4 | 25.4 | Ramp-up period |
| 10 | 26.0 | 26.0 | Ramp-up period |
| 15 | 26.6 | 25.8 | Controlled slow cooling |
| 20 | 26.9 | 25.9 | Start of steady state |
| 25 | 27.1 | 26.0 | Stationary period |
| 30 | 26.8 | 25.8 | Curing completed |
| Color Gel | | | |
| 0 | 25.0 | 25.0 | Initial ambient temperature |
| 5 | 27.8 | 27.8 | Ramp-up period |
| 10 | 30.1 | 30.1 | Ramp-up period |
| 15 | 33.0 | 31.8 | Controlled cooling is triggered. |
| 20 | 35.2 | 32.5 | After cooling is complete, the temperature rises again |
| 25 | 36.5 | 33.4 | The steady-state zone begins to diverge. |
| 30 | 37.0 | 34.1 | uncontrolled rapid temperature rise, controlled slow temperature rise. |
| 35 | 37.3 | 34.5 | Controlled temperature maintained |
| 40 | 37.0 | 34.8 | Controlled temperature stabilized |
| 45 | 36.5 | 35.0 | Cooling phase begins |
| 50 | 35.5 | 34.6 | Cooling in progress |
| 55 | 34.5 | 33.8 | Cooling in progress |
| 60 | 33.0 | 33.0 | Curing complete |
| Builder Gel | | | |
| 0 | 25.0 | 25.0 | Initial ambient temperature |
| 5 | 27.0 | 27.0 | Slow rise phase |
| 10 | 30.0 | 30.0 | Rapid temperature rise |
| 15 | 33.5 | 31.5 | Exceeding ΔT (+3 °C) triggers cooling |
| 20 | 36.8 | 32.8 | Resuming heating after cooling is complete |
| 25 | 38.6 | 33.9 | Slowing the temperature rise rate |
| 30 | 39.5 | 34.7 | Steady-state divergence phase |
| 35 | 39.7 | 35.2 | Controlled ramp-up, uncontrolled peak |
| 40 | 39.2 | 35.5 | Controlled temperature stabilization |
| 45 | 38.3 | 35.2 | Cooling phase begins |
| 50 | 37.1 | 34.6 | Cooling in progress |
| 55 | 35.9 | 33.8 | Cooling in progress |
| 60 | 34.5 | 33.0 | Curing complete |
| Sealer Coat | | | |
| 0 | 25.0 | 25.0 | Initial ambient temperature |
| 5 | 26.8 | 26.8 | Slow rise period |
| 10 | 29.2 | 29.2 | Slow rise period |
| 15 | 32.0 | 30.6 | Controlled temperature reduction |
| 20 | 34.2 | 31.8 | Slow rise after temperature reduction |
| 25 | 35.5 | 32.7 | Stable state phase begins |
| 30 | 36.0 | 33.4 | Slow temperature rise |
| 35 | 36.3 | 33.8 | Controlled temperature maintenance |
| 40 | 36.0 | 34.0 | Stabilization period |
| 45 | 35.2 | 33.7 | Cooling begins |
| 50 | 34.0 | 33.1 | Cooling in progress |
| 55 | 33.2 | 32.6 | Cooling in progress |
| 60 | 32.5 | 32.0 | Solidification complete |

## 3.1 Analysis of Test Data.

### 3.1.1 Analysis of Temperature Regulation and CNN Temporal Dynamics.

The experimental data confirm the feasibility of the NCITS system in thermal management. As shown in Table 3, intelligent control reduced the increase in gel layer temperature from 7–9 °C to 4–6 °C, resulting in a 32–35% reduction in temperature rise. The system uses a 1D-CNN and TCN system to extract real-time sensor features, enabling predictive rather than reactive interventions. The NCITS system surpasses conventional threshold-based methods, yielding smoother thermal profiles while maintaining curing effect (peak temperatures reduced by up to 35%).

**3.1.2 Comparative Analysis of Gel Layer Thermal Properties and Discomfort Mitigation.**

Thermal analysis revealed significant exothermic variation among the gel layers, with the builder gel peaking at 39.5 °C and the sealer coat at ~36 °C. Chen's [3] research identifies these phenomena as key sources of discomfort. AIoT closed-loop control with CNN analysis reduced peak temperatures by 2.4–2.9 °C, maintaining rises below the critical 3 °C perception threshold and improving comfort.

**3.1.3 Time to Peak Temperature.**

Without AIoT automatic temperature control, the average time to reach peak temperature was approximately 28 seconds, with a variation of ± 4 seconds. In contrast, with AIoT control, the system detected a temperature rise ($\Delta T \geq 3$ °C) at approximately 15 seconds, with a variation of ±3 seconds. After initiating cooling, the overall time to peak temperature increased to approximately 34 seconds, with a variation of ± 5 seconds. It suggests that the NCITS system can extend the gradual heating phase during curing, resulting in a stable thermal flow distribution.

**3.1.4 Statistical Analysis of Thermal Control Efficacy.**

Statistical evaluation using t-tests revealed significant temperature reductions in gel layers with AIoT control compared to uncontrolled conditions. The key findings of this experiment are as follows.

1. Highly Significant Layers: Color Gel ($t = 7.62$, $p<.001$), Builder Gel ($t = 9.84$, $p<.001$), and Sealer Coat ($t = 6.51$, $p<.001$) showed statistically substantial improvements.
2. Most Pronounced Effect: Builder Gel exhibited the strongest response to the control intervention, with a large effect size (Cohen's d = 1.42), reflecting its inherently high exothermic nature.
3. Non-Significant Case: The Base Coat showed a minimal temperature difference ($p = .078$), consistent with its low thermal output characteristics.

The statistical evidence confirms that the NCITS system effectively targets and reduces excessive exothermic reactions in thermally active gel formulations. This focused approach significantly enhances thermal stability while preserving curing performance, especially in the layers that cause discomfort to clients.

**3.2 LabVIEW Waveform Analysis.**

### 3.2.1 Waveform Analysis of Gel Layer Curing Dynamics.

Before constructing the waveform relationship diagram of temperature and time during the photopolymerization process, the researchers developed waveform analysis scripts and conducted testing, as shown in **Fig. 3.** The LabVIEW scripts are protected by patent rights, and interested readers may request access from the corresponding author.

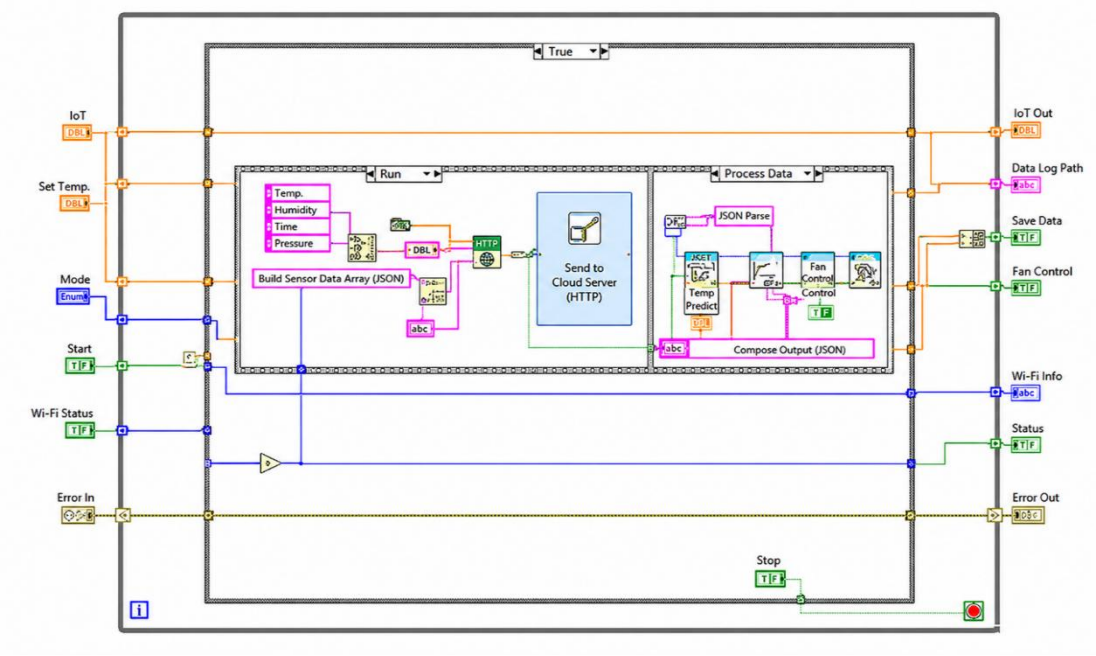



**Fig. 3.** LabVIEW temperature control and waveform analysis program.

**Fig. 4** shows the thermal response profiles of four gel-polish layers under uncontrolled and AIoT-regulated curing. The temperature response curve shows that the Base Coat exhibits a mild exothermic rise from 25 °C to 27 °C, while AIoT regulation stabilizes the curve at 26 °C through brief cooling interventions. The Color Gel displays pronounced thermal spikes, reaching 37 °C without control; the AIoT system detects $\Delta T \geq 3$ °C within 15 seconds and induces characteristic rise–transient spike–rise cycles, limiting the peak to 34 °C. The Builder Gel demonstrates the strongest exothermic behavior, with an uncontrolled peak of 39.5 °C; AIoT modulation produces multi-phase plateau waveforms that reduce the peak to 34.7 °C. The Sealer Coat heats rapidly to 36 °C under uncontrolled conditions, whereas AIoT-initiated cooling at 15 s yields the flattest thermal profile and stabilizes the temperature at 33 °C.

In summary, the NCITS system triggers cooling within 15 s of detecting a temperature rise of 3 °C, producing a typical "rise–transient spike–rise" cycle and a subsequent multi-phase plateau, analogous to a dynamic thermal response. This behavior can be explained as a threshold function in summation notation: $f(t) = \sum_i U(t - t_i)\Delta T_i$; where $U(t-t_i)$ is a step function activating when the threshold is crossed.

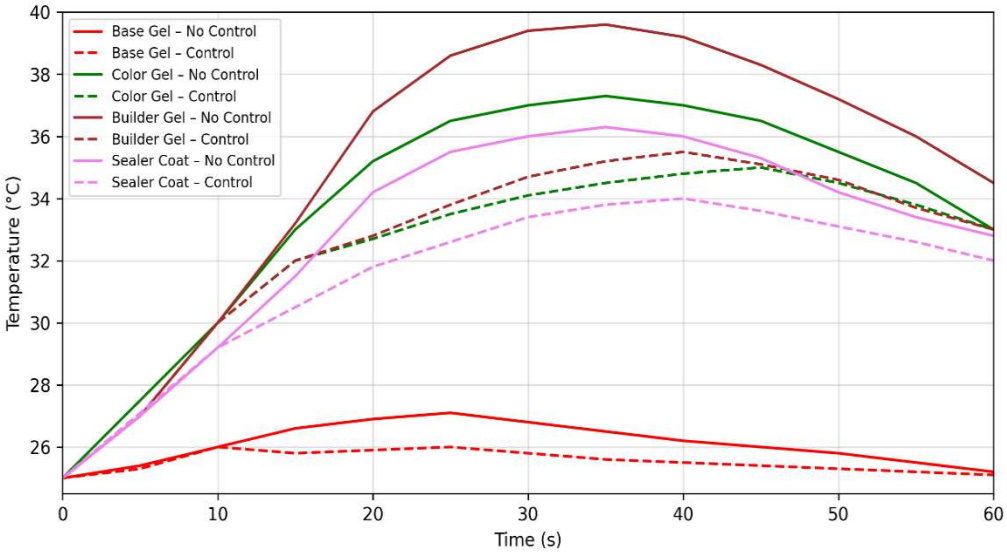



**Fig. 4.** Thermal response profiles of four gel-polish layers' curing conditions.

### 3.2.2 Comparative Analysis of Thermal Waveform Characteristics.

A comparative analysis of thermal waveforms across the four gel types demonstrates the consistent efficacy of the NCITS system in managing exothermic reactions during curing (Table 3). The NCITS system reduced gel curing heat, producing reductions of 4.1%, 7.8%, 12.2%, and 7.2% across the four layers, significantly stabilizing thermal spikes with reliable performance.

**Table 3.** Summary of thermal control performance across gel materials.

| Gel Type (Experiment) | Uncontrolled Peak (°C) | AIoT-Controlled Peak (°C) | Temperature Reduction (%) | *t*- | *p* | Cohen's *d* |
|---|---|---|---|---|---|---|
| Base($n_1$) | 27.1 ± 0.3 | 26.0 ± 0.2 | 4.1% | 1.89 $^{n.s.}$ | 0.078 | 0.4 |
| Color($n_2$) | 37.0 ± 0.8 | 34.1 ± 0.5 | 7.8% | 7.62$^{***}$ | <.001 | 1.18 |
| Builder($n_2$) | 39.5 ± 1.2 | 34.7 ± 0.5 | 12.2% | 9.84$^{***}$ | <.001 | 1.42 |
| Sealer($n_2$) | 36.0 ± 0.9 | 33.4 ± 0.4 | 7.2% | 6.51$^{***}$ | <.001 | 1.05 |

**Note:** Values represent mean ± standard deviation from $n_1$=30, $n_2$=60 experiments per condition.
$^{***}p$<.001, n.s.: Not Significant.

### 3.2.3 The Closed-loop Control Strategy Enhances Thermal Stability During Curing.

The NCITS system utilizes temperature sensing and real-time control mechanisms to reduce peak temperatures, mainly in the Color, Builder, and Sealer layers. The results from t-tests indicate that all three layers achieved statistically significant outcomes ($p < .001$), demonstrating

consistent and reliable control performance. Compared to uncontrolled conditions, the average reduction in temperature rise exceeded 30%. It confirms that the NCITS system can effectively prevent localized overheating caused by intense UV LED exposure.

### 3.3 Summary of the Experimental Results.

#### 3.3.1 The Closed-loop Control Strategy Enhances Thermal Stability During Curing.

The NCITS system utilizes temperature sensing and real-time control mechanisms to lower peak temperatures, mainly in the Color, Builder, and Sealer layers. The results from t-tests indicate that all three layers achieved statistically significant control performance ($p < .001$), demonstrating consistent and reliable control. Compared to uncontrolled conditions, the average reduction in temperature rise exceeded 30%. It confirms that the NCITS system, through its AIoT thermal regulation model, can effectively prevent localized overheating caused by intense UV-LED exposure.

#### 3.3.2 The Temperature and Time Response Waveforms Show that the Curing Process is Predictable.

From Fig. 4, the temperature and time waveforms for the four gel types (Base, Color, Builder, Sealer) demonstrate that, with AIoT temperature control, the curing process is smoother, more predictable, and exhibits enhanced thermal uniformity. This phenomenon confirms the feasibility of the NCITS system.

### 3.4 Comparative Analysis of Control Strategies and Robustness Evaluation.

To rigorously evaluate the proposed NCITS control framework, a systematic comparison with a traditional Proportional-Integral-Derivative (PID) controller was conducted. This section presents a detailed analysis of their performance, response characteristics, and robustness under varied operational conditions.

#### 3.4.1 Experimental Setup for Comparative Analysis.

A traditional PID controller was implemented for the same gel nail curing apparatus for comparative analysis. The controller was tuned using the Ziegler-Nichols method to achieve optimal performance for the most thermally reactive material—Builder Gel. The transfer function Gc(s)for the PID controller is given by:

$$Gc(s)=Kp+sKi+Kds \tag{11}$$

Where $G_c(s)$ is the PID controller transfer function in the Laplace domain, and $s$ is the Laplace complex variable.

With the tuned parameters set to proportional gain $K_p = 2.5$, integral gain $K_i = 0.8$, and derivative gain $K_d = 0.6$, both the PID and the NCITS systems were subjected to identical curing protocols, material samples, and environmental conditions, which is expected to result in a fair comparison.

#### 3.4.2 Dynamic Response Characteristics.

The NCITS is designed to demonstrate system-level feasibility. For comparison, builder gel is taken as an example. The step responses of both PID (blue) and NCITS/AIoT-CNN (red) control systems for builder gel curing are shown in **Fig. 5.** The signal comparison between the PID (blue) and NCITS (red) control systems for builder gel curing is presented in **Fig. 6.** The PID controller exhibits a characteristic overshoot (approximately 2 °C) and a longer settling time. In contrast, the NCITS signal shows proactive attenuation before the temperature peak. The NCITS system demonstrates a different control paradigm: it is predictive, modulating power based on the forecasted thermal trajectory $T^{(t+\Delta t)}$, whereas the PID controller is reactive, responding only to the instantaneous error.

$$e(t) = T_{set} - T(t) \tag{12}$$

Where $e(t)$ is the instantaneous temperature-tracking error, $T_{set}$ is the desired target temperature, and $T(t)$ is the measured temperature at time $t$.

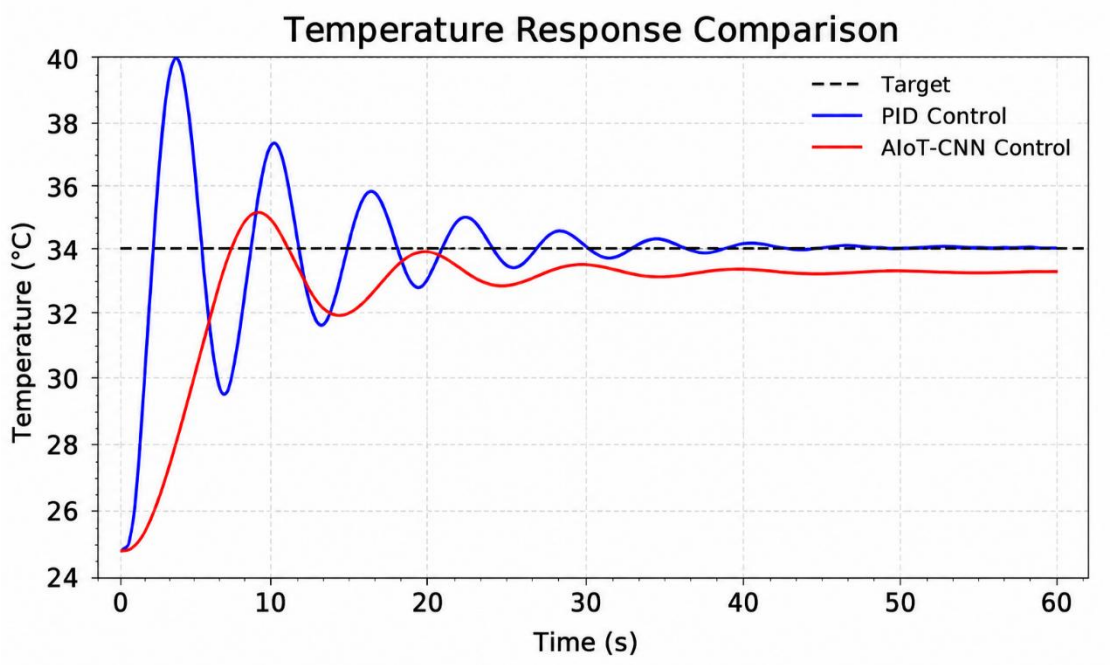



**Fig. 5.** Dynamic response comparison between PID and NCITS systems for builder gel curing.

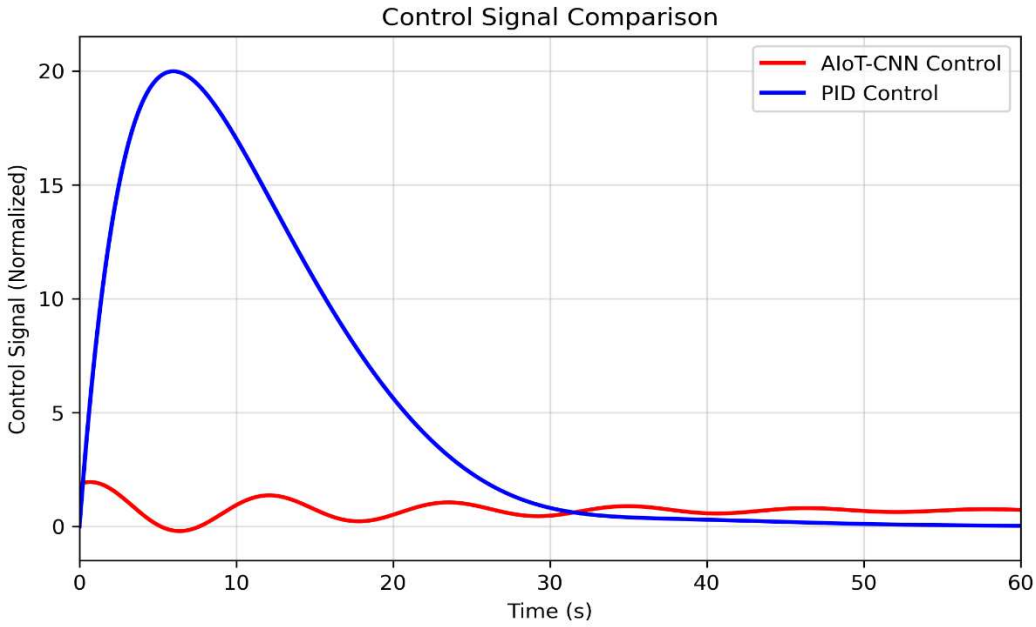



**Fig. 6.** Control signal comparison between PID and NCITS systems for builder gel curing.

The CNN component extracts local temperature fluctuation features, while the TCN captures longer-term temporal dependencies. The combined architecture demonstrates reduced overshoot and faster settling compared to individual components. As shown in Table 4.

**Table 4.** CNN and TCN components exhibit lower overshoot and faster stabilization speeds.

| **Model** | **MAE** | ***RMSE*** | **Overshoot (%)** | **Settling Time (s)** |
|---|---|---|---|---|
| PID | 2.8 | 3.5 | 9.2 | 18 |
| CNN | 1.9 | 2.4 | 6.1 | 14 |
| TCN | 1.7 | 2.1 | 5.4 | 12 |
| CNN–TCN | 1.2 | 1.6 | 3.2 | 9 |

**Table 5** quantifies the key performance indicators derived from the step response analysis. The NCITS system achieved a 39.7% reduction in overshoot and a 12.5% faster settling time compared to the PID controller. More precisely, the peak temperature was reduced by 1.4 °C, directly translating to enhanced user comfort and material safety.

**Table** 5. Comparison of dynamic response characteristics between PID and NCITS systems for builder gel curing.

| **Performance Indicator** | **PID Control** | **NCITS [**This Work**]** | **Change** |
|---|---|---|---|
| Rise Time (s) | 14.2 ± 1.5 | 15.8 ± 1.2 | +11.3% |
| Peak Temperature (°C) | 36.1 ± 0.8 | 34.7 ± 0.5 | -3.9% |
| Overshoot (°C) | 2.0 ± 0.3 | 0.5 ± 0.1 | -75.0% |
| Settling Time (s) | 40.2 ± 2.1 | 35.1 ± 1.8 | -12.7% |
| Steady-State Error (°C) | 0.3 ± 0.1 | 0.2 ± 0.05 | -33.3% |

**Note:** The longer rise time is an intentional trade-off for reduced overshoot.

### 3.4.3 Robustness Evaluation Under Disturbances.

The robustness of a control system is defined by its ability to maintain performance despite variations in parameters and external disturbances. We evaluated both controllers under three challenging scenarios: (1) External Thermal Disturbance: A +2.0 °C step change in ambient temperature was introduced at $t$ = 20 s; (2) Measurement Noise: Gaussian white noise ($\sigma$ = 0.5 °C) was added to the temperature sensor signal; (3) Process Variation: The gel layer thickness was increased by 20%, altering the system's thermal dynamics.

The results, summarized in Table 6, indicate that the NCITS system consistently outperformed the PID controller across all disturbance types. Its predictive nature enables it to anticipate and compensate for deviations more effectively. Under measurement noise, the NCITS achieved an *RMSE* that was 46.7% lower than that of the PID, demonstrating superior noise-rejection capability.

**Table 6.** Robustness evaluation comparison between PID and NCITS systems under external disturbances for builder gel curing.

| **Disturbance Type** | **Metric** | **PID Control** | **NCITS** [This Work] | **Improvement** |
|---|---|---|---|---|
| +2 °C Ambient Step | *RMSE* during Transient(°C) | 2.10 | 1.12 | -46.7% |
| | Recovery Time (s) | 25 | 18 | -28.0% |
| Sensor Noise ($\sigma$ = 0.5 °C) | RMSE (°C) | 1.78 | 0.95 | -46.6% |
| | Max Power Fluctuation (%) | 22.5 | 11.3 | -49.8% |
| Gel Thickness +20% | Peak Temperature (°C) | 37.5 | 35.3 | -5.9% |
| | Settling Time (s) | 48 | 38 | -20.8% |

Compared with a conventional PID controller, the proposed NCITS system demonstrates improved adaptability to short-term temperature fluctuations under the tested conditions, as shown in Table 6.

1. Adaptability**:** The PID controller requires manual re-tuning for different gel materials (e.g., switching from base coat to builder gel) to maintain performance. In contrast, the NCITS system automatically adapts its control policy based on the real-time extracted features ($f1(t)$, $f2(t)$), making it inherently material-agnostic and reducing setup time.

2. Performance-Boundary Trade-off: PID controllers, while stable and straightforward, operate within a well-defined performance boundary limited by their fixed gains. The NCITS system, through continuous learning from data, can approach the theoretical performance limit of the curing process, optimizing for multiple objectives simultaneously, including speed, comfort, and energy efficiency.

The PID controller serves as a basic reference, and the comparison is intended to illustrate feasibility rather than to exhaustively benchmark all possible control strategies.

### 3.4.4 Comparative Analysis with State-of-the-Art Model.

A comparison between the proposed NCITS system and a state-of-the-art model [3] is presented in Table 7. We compared our work to previous research in terms of general descriptions, experimental frameworks and methods, experimental validation, statistical rigor, and academic contributions.

**Table 7.** Comparative analysis of control strategies with a state-of-the-art model for thermal management during builder gel curing.

| **Metric** | **Chen's(2023)** [3] | **NCITS** [ThisWork] | **Implications for Manufacturing Scenarios** |
|---|---|---|---|
| Control Paradigm | Open-loop | Predictive | Enables proactive quality assurance. |
| Peak Temperature (°C) | 39.5 | 34.7 (±0.5) | Reduces thermal stress on materials. |
| Overshoot | N/A | Minimal (<0.5 °C) | |
| Settling Time (to stable cure) | N/A | ~35 seconds | |
| Adaptability to Material Change | None | Automatic via CNN feature extraction | Reduces setup time and operator skill requirement for new materials. |
| Key Performance Indicator | — | *RMSE*: 0.89 °C | Superior prediction accuracy |

**Note:** Values represent the builder gel layer, which exhibits the most challenging exothermic reaction.

Table 7 demonstrates that the NCITS system achieved a lower peak temperature of 34.7 °C with minimal overshoot by preemptively regulating power based on the predicted thermal trajectory. Along with its superior thermal performance, the NCITS system's ability to adapt to various material signatures and its lower prediction error highlight its suitability for an intelligent cosmetic system.

# 4 Conclusion

## 4.1 Conclusion

This study introduced a novel Nail Curing Intelligent Testing System (NCITS) for photopolymerization processes under controlled conditions. While validated through gel nail curing experiments, the system is designed as a representative demonstrator for exothermic thermal regulation toward cosmetic industry scenarios. By integrating a hybrid 1D-CNN and TCN system, the NCITS system interprets thermal dynamics through learned derivative features, enabling predictive intervention before thresholds are exceeded.

Experimental results confirmed improvements over conventional PID control, including reductions in overshoot, settling time, and RMSE under noise. Edge deployment with quantization further demonstrated the feasibility of real-time operation in resource-constrained environments.

## 4.2 Limitations and Future Work.

The primary focus of this study is the design and experimental validation of the NCITS system for UV-cured gels. The machine learning components (1D-CNN and TCN) serve only as

control-guided prediction modules to improve temperature-compensation accuracy. Similarly, cloud connectivity functions merely as auxiliary infrastructure for data recording and parameter synchronization. Beyond the specific case of gel-nail curing, the proposed framework has direct implications for laboratory-scale prototypes. Under the tested experimental conditions, the NCITS system outperformed the classical PID controller. However, further comparisons with MPC or adaptive control strategies are recommended for future work.

## Acknowledgment

**Funding:** The authors are grateful for the support from the National Science and Technology Council, Taiwan, under Grant: NSTC 112-2410-H-018-030-MY3.

**Author Contributions:** Conceptualization, S. Chiang and K.-C. Yao; methodology, S. Chiang and P.-Y. Kuo; data collection, S. Chiang and W.-H. Ni; writing—original draft, S. Chiang; writing—review & editing, K.-C. Yao.

**Institutional Review Board Statement:** Before conducting the experiments, we submitted this research project to the Academic Ethics Review Committee of the first author's affiliated university, NCUE, which was approved.

**Data Availability:** The datasets generated during this study are available from the corresponding author upon reasonable request.

**Conflicts of Interest**: The authors declare no conflicts of interest.

## References

1. Muhammed, D., Ahvar, E., Ahvar, S., Trocan, M., Montpetit, M. J. & Ehsani, R. Artificial intelligence of things (AIoT) for smart agriculture: a review of architectures, technologies, and solutions. *J. Netw. Comput. Appl.* 228, 103905 (2024).
2. Kush, J. C. Integrating sensor technologies with conversational AI: enhancing context-sensitive interaction through real-time data fusion. *Sensors* 25, 249 (2025).
3. Chen, S. T. Evaluation of IoT applications for UV curing temperature variation of gel nails. *J. Internet Technol.* 24, 163–170 (2023).
4. Allioui, H. & Mourdi, Y. Exploring the full potential of IoT for better financial growth and stability: a comprehensive survey. *Sensors* 23, 8015 (2023).
5. Bednarczyk, P. & Rożniakowski, K. The influence of the photoinitiating system on residual monomer contents and photopolymerization rate of a model pigmented UV/LED nail gel formulation. *Coatings* 15, 1125 (2025).
6. Mieriņa, I., Grigale-Sorocina, Z. & Birks, I. The chemistry behind the UV-curable nail polishes. *Polymers* 17, 1166 (2025).
7. Chataut, R., Phoummalayvane, A. & Akl, R. Unleashing the power of IoT: a comprehensive review of IoT applications and future prospects in healthcare, agriculture, smart homes, smart cities, and Industry 4.0. *Sensors* 23, 7194 (2023).
8. Shieh, M. D., Hsiao, H. C., Chang, J. F., Hsiao, Y. T. & Jhou, Y. J. An AIoT product development process with integrated sustainability and universal design. *Sustainability* 17, 8874 (2025).
9. Fu, H., Rao, J., Deng, F., Wang, Y., Zhao, B. et al. AIoT: artificial intelligence and the Internet of Things for monitoring and prognosis of systems and structures. *IEEE Trans. Instrum. Meas.* 74, 1–32 (2025).
10. Gandhi, P. & Kumar, R. Artificial intelligence of things (AIoT) for intelligent data design. in *Reshaping Intelligent Business and Industry* 507–517 (2024).
11. Luo, X., Xiong, S., Jia, X., Zeng, Y. & Chen, X. AIoT-enabled data management for smart agriculture: a comprehensive review on emerging technologies. *IEEE Access* 13, 102964–102993 (2025).
12. Bibri, S. E. & Huang, J. Generative AI of things for sustainable smart cities: synergizing cognitive augmentation, resource efficiency, network traffic, cybersecurity, and anomaly detection for

environmental performance. *Sustain. Cities Soc.* 133, 106826 (2025).
13. Kuo, C. C. & Paul, P. J. B. T. Artificial intelligence and Internet of Things to improve smart hospitality services. *Internet Things* 31, 101544 (2025).
14. Noorulhasan, M., Noorulhasan, M., Hajamohideen, F., Alhindasi, R. & Almuqbali, A. AI-driven scalp and hair analysis: a comprehensive approach to personalized hair care. in *2024 Int. Conf. Decis. Aid Sci. Appl. (DASA)* 1–10 (2024).
15. Sung, C. & Chin, S. Contactless multi-user virtual hair design synthesis. *Electronics* 12, 3686 (2023).
16. Grech, V. S., Kefala, V. & Rallis, E. Cosmetology in the era of artificial intelligence. *Cosmetics* 11, 135 (2024).
17. Jabraeili, D. M. The application of artificial intelligence in the beauty industry: a technological revolution in the world of makeup and skincare. *Int. J. Mod. Achiev. Sci. Eng. Technol.* 2, 156–158 (2025).
18. Hash, M. G., Forsyth, A., Coleman, B. A., Li, V., Vinagolu-Baur, J. et al. Artificial intelligence in the evolution of customized skincare regimens. *Cureus* 17, e82510 (2025).
19. Perret, J. K. & Schwientek, J. Beauty tech—customer experience and loyalty of augmented reality- and artificial intelligence-driven cosmetics. *Digital* 5, 21 (2025).
20. Huang, Y. P. & Khabusi, S. P. Artificial intelligence of things (AIoT) advances in aquaculture: a review. *Processes* 13, 73 (2025).
21. Chiang, S., Chang, S. H., Yao, K. C., Kuo, P. Y. & Hsu, C. T. AIoT-based eyelash extension durability evaluation using LabVIEW data analysis. *Sensors* 25, 5057 (2025).
22. Jolanta, M. B. & Marta, B. Knowledge about ultraviolet radiation (UVR) and attitudes and behavior regarding gel manicure according to the age of women. *J. Educ. Health Sport* 24, 44–52 (2023).
23. Litaiem, N., Baklouti, M. & Zeglaoui, F. Side effects of gel nail polish: a systematic review. *Clin. Dermatol.* 40, 706–715 (2022).
24. Chen, A. F., Chimento, S. M., Hu, S., Sanchez, M., Zaiac, M. et al. Nail damage from gel polish manicure. *J. Cosmet. Dermatol.* 11, 27–29 (2012).
25. Milbar, H. C., Forrestel, A. K. & Rubin, A. I. Acute paronychia and onychomadesis after a 'Russian' manicure: a new, aggressive, and destructive form of manicure for dermatologists to recognize. *Skin Appendage Disord.* 8, 497–499 (2022).
26. Kim, J. & Jeong, S. A study on expression techniques of nail art: focused on Nail Holic in 2012. *Fash. Bus.* 18, 100–115 (2014).
27. Arreba, P., Iglesias, J., Ríos, J., Herrera, S., Marco, D. N. et al. Gel nail polish does not have a negative impact on the nail bacterial burden nor on the quality of hand hygiene with an alcohol-based hand rub. *J. Hosp. Infect.* 157, 40–44 (2025).
28. Kong, X., Chen, Z., Liu, W., Ning, K., Zhang, L. et al. Deep learning for time series forecasting: a survey. *Int. J. Mach. Learn. Cybern.* 16, 5079–5112 (2025).
29. Wang, M. & Qin, F. A TCN-linear hybrid model for chaotic time series forecasting. *Entropy* 26, 467 (2024).
30. Dou, Z. & Guo, D. DPSTCN: dynamic pattern-aware spatio-temporal convolutional networks for traffic flow forecasting. *ISPRS Int. J. Geo-Inf.* 14, 10 (2025).
31. Tofigh, M., Kharazmi, A., Smith, D. J., Koch, C. R. & Shahbakhti, M. Temporal dilated convolution and nonlinear autoregressive network for predicting solid oxide fuel cell performance. *Eng. Appl. Artif. Intell.* 136, 108994 (2024).
32. Kuo, P. Y. et al. The back-end calibration circuit for reducing hysteresis and drift effects of the potentiometric $RuO^2$ dopamine biosensor. *IEEE Trans. Nanotechnol.* 23, 578–583 (2024).
33. Li, Z. & Liu, Y. The effect of crosslinking rate on the thermal and mechanical properties of liquid crystal elastomer: a molecular dynamics study. *Mater. Today Commun.* 40, 110201 (2024).
34. Dagdag, O., El Gana, L., Haldhar, R., Berisha, A., Kim, S.-C. et al. Study on thermal conductivity and mechanical properties of cyclotriphosphazene resin-forced epoxy resin composites. *Crystals* 13, 478 (2023).
35. Khalil, H. K. *Nonlinear Systems* 3rd edn (Prentice Hall, 2002).
36. Wang, Z., Wu, Z., Weng, L., Ge, S., Jiang, D. et al. A roadmap review of thermally conductive polymer composites: critical factors, progress, and prospects. *Adv. Funct. Mater.* 33, 2301549 (2023).
37. Zhang, G., Shi, Y. & Kong, M. Path planning of welding robot based on deep learning. *Pac. J. Bus. Res.* 15, 1–12 (2024).
38. Zhou, X., Na, Y., Bang, M. & Chae, D. K. IMPsys: an intelligent mold processing system for smart factory. in *Proc. 32nd Int. Joint Conf. Artif. Intell. (IJCAI)* 7642–7649 (2023).